Soft Matter

PAPER

View Article Online
View Journal | View Issue

Cite this: *Soft Matter*, 2020, **16**, 10921

Universality in coalescence of polymeric fluids†

Sarath Chandra Varma,[a] Aniruddha Saha,[b] Siddhartha Mukherjee,[bc] Aditya Bandopadhyay,[b] Aloke Kumar [a] and Suman Chakraborty *[bc]

Received 15th September 2020,
Accepted 18th October 2020

DOI: 10.1039/d0sm01663b

rsc.li/soft-matter-journal

A pendant drop merging with a sessile drop and subsequently forming a single daughter drop is known to exhibit complex topologies. But their dynamics are yet to be probed for fluids exhibiting characteristic relaxation time scales while undergoing the deformation process. Here, we unveil a universal temporal evolution of the neck radius of the daughter drop during the coalescence of two polymeric drops. Such a generalization does not rely on the existence of previously explored viscous and inertial dominated regimes for simpler fluids but is fundamentally premised on a unique topographical evolution with essential features of interest exclusively smaller than the dominant scales of the flow. Our findings are substantiated by a theoretical model that considers the drops under coalescence to be partially viscous and partially elastic in nature. These results are substantiated with high-speed imaging experiments on drops of polyacrylamide (PAM), polyvinyl alcohol (PVA), polyethylene oxide (PEO), and polyethylene glycol (PEG). The observations herein are expected to hold importance for a plethora of diverse processes ranging from biophysics and microfluidics to the processing of materials in a wide variety of industrial applications.

1 Introduction

The process of merging of two or more drops in proximate contact to merge and form a single daughter drop is ubiquitous in natural phenomena such as raindrop condensation,[1–4] and industrial phenomena such as spraying,[5] coating,[6] condensation of droplets on surfaces[7] and even processes linked to life itself.[8–11] In the atmospheric realm, collision and coalescence of water drops have been identified as key ingredients towards the growth of raindrops and the evolution of thunderstorms.[12] In industrial processes, the coalescence of droplets occurs in a plethora of diverse applications. For example, in the petroleum industry, it is associated with dispersed water removal and oil desalting.[13] In the food industry, it holds the key to deciding the shelf life of emulsion-based products such as salad dressing and mayonnaise.[14] It also occurs in dense spray systems and combustion.[15] In materials processing, sintering of spherical particles closely mimics the processes of coalescence of complex fluid droplets.[16] In more recent times, droplet coalescence in liquid crystals,[17] emulsions,[18–20] particle deposition,[21] interfacial rheology[22] and in microfluidic devices[23] have opened up new possibilities in chemistry, biological and materials sciences. Despite the applications of drop coalescence being fascinating, rich, and scientifically diverse, a unification of the underlying physics through universally applicable scaling law, beyond Newtonian fluids, remains to be an elusive proposition.

The temporal evolution of the liquid neck at the junction of coalescing drops is initially modulated solely by the Laplace pressure so that the sudden change in topology when the two drops become unified may be linked with a unique dynamical singularity.[24] This, besides, is featured with an exclusive separation of scales as the essential dimensional features of interest turn out to be significantly smaller than the dominant scales of the flow.[25] For Newtonian drops, the entire dynamical evolution during coalescence has been identified to be associated with a dominating viscous regime at sufficiently early stages,[26] and an inertial regime at later instances.[25] Apart from the inertial and viscous regimes, a new regime of inertially limited viscous regime[27] was demonstrated which highlights the distinction of the inertial variation[25] of $R \propto t^{0.5}$ from the proposed linear variation[27] of the neck radius R with time t. Off late, an additional initial asymptotic regime has been unveiled, where the inertial, viscous, and surface tension forces are all important.[26] Such a complex interplay of events, however, makes it extremely difficult, if not impossible, to portray any universality in the dynamics of coalescing droplets over the entirety of experimentally meaningful temporal spans.

In the literature, regime-wise universality in droplet coalescence has been demonstrated, both experimentally and

[a] *Department of Mechanical Engineering, Indian Institute of Science, Bengaluru, Karnataka-560012, India. E-mail: alokekumar@iisc.ac.in; Tel: +91 80-22932958*
[b] *Department of Mechanical Engineering, Indian Institute of Technology Kharagpur, West Bengal-721302, India*
[c] *Advanced Technology Development Center, Indian Institute of Technology Kharagpur, West Bengal-721302, India. E-mail: suman@iitkgp.mech.ac.in; Tel: +91 3222-282990*

† Electronic supplementary information (ESI) available. See DOI: 10.1039/d0sm01663b

analytically[24–26,28–42] for Newtonian fluids. For such drops, it has been established that the kinematics of the phenomenon is governed by the growth of the liquid bridge that can be typically characterized by the temporal change of the neck radius. In the viscous dissipation dominated regime, the neck radius evolution has been shown to follow: $R^* \sim t^* \ln(t^*)$, where R^* (neck radius non dimensionalized by initial radius of drop R_o) and t^* (normalized time with viscous time scale $\tau_v = \eta R_o/\sigma$ where η is viscosity and σ is surface tension) being the relevant dimensionless parameters.[32,33,43,44] In the inertia dominated regime for Newtonian fluids, it has been shown that the radius scales as $R^* \sim (t^*)^{1/2}$, where t^* is the time normalized with inertial time scale $\tau_i = \left(\frac{\rho R_0^3}{\sigma}\right)^{\frac{1}{2}}$,[24] ρ being the density.

The paradigm of a possible universal depiction of collision dynamics, however, becomes significantly more involved as rheologically complex fluids are considered to coalesce. For example, polymeric fluids, which are a distinct sub-set of viscoelastic fluids, contain macromolecules that can exhibit strongly non-Newtonian characteristics such as polymer chain entanglements and molecular relaxations,[45] characterized by the relevant spatial and temporal scales. Polymers for which water acts as a good solvent such as polyacrylamide (PAM) and polyethylene oxide (PEO), among others, admit various states of polymer chain interactions depending on the level of dilution of the polymer. The co-existence of viscoelastic relaxations along with dissipative and inertial dynamics introduces additional complexity so that the constitutive relations may or may not admit universal solutions. Under such conditions, the possible existence of universal dynamics characterizing droplet coalescence phenomenon over experimentally realizable physical scales remains to be an open question.

Here, we demonstrate that for aqueous solutions of polymers, coalescence of a sessile and a hanging pendant drop can be characterized by a universal scaling relationship. To experimentally depict the underlying universality, we study the coalescence of droplets of four different water-soluble polymers: polyacrylamide (PAM), polyethylene oxide (PEO), polyvinyl alcohol (PVA), and polyethylene glycol (PEG). By investigating coalescence phenomenon for aqueous solutions of the polymers, which we call rheocoalescence, at various concentrations varying from dilute to semi-dilute entangled regimes, we unveil a universal temporal evolution of the necking radius of polymeric fluid drops. Experimental observation of a universal regime for these polymeric fluids is also supported by scaling analysis based on a linear Phan-Thien-Tanner (PTT) model.[46] Our results stand in strong contrast to the universality found in Newtonian fluids and hold enormous promise for opening new paradigms in rheological measurements.

2 Experiments

Polymer solutions are prepared by dissolving enough quantity of polymer to distilled water (DI water) to get 0.2%, 0.3%, 0.4%, 0.5% and 0.6% w/v concentrations c of all chosen polymers. For PAM we have additional concentrations of 0.01%, 0.02%, 0.04%, 0.05%, and 0.06%. We also have PEG with concentrations of 8%, 12%, 16%, 20%, and 24%. All the above solutions are agitated at 1200 rpm at room temperature for different durations except PVA. The list of molecular weights, time taken to prepare the solution, and the suppliers of the polymers used are provided in Table 1. Concentrations of the polymers are chosen in a way that the solutions types vary in a range of dilute, semi-dilute unentangled, and semi-dilute entangled regimes. The semi dilute unentangled and semi dilute entangled regimes are differentiated using entanglement concentration c_e which is 5–10 times of critical concentration c^*.[47,48] For PAM, the entanglement concentration is given as $c_e \approx 9c^*$.[49] Similarly, the entanglement concentration for PEO is $c_e \approx 6c^*$.[50] Concentrations of 0.5% and 0.6% are chosen for PEO, and 0.6% for PAM for the experiments are in semi-dilute entanglement regime.

Coalescence is achieved by dispensing a drop of 2 mm diameter on a substrate with a pendant drop of the same size, lowered by a Z-stage with an approach velocity $\sim 10^{-4}$ m s^{-1} to ensure the drops to coalesce in a controlled manner. The experiments have been performed at standard temperature and pressure of 25 °C and 1 atm respectively. The schematic of the experimental setup is shown in Fig. 1a. The coalescence is imaged with Vision Research v641 high-speed camera at 90 000 frames per second using Zoom7000 Navitar lens mounted in front of the droplets with illumination using light-emitting diode optical source. Image analysis is performed using MATLAB.

Surface tension values, σ, of the polymeric solutions are measured using Optical contact angle measuring and contour analysis systems (OCA25) instrument from Dataphysics by the pendant drop method. Density ρ of the solutions was obtained by measuring the mass and volume and was found to be very close to that of water with a value of 1000 ± 50 kg m^{-3}. This leads us to assume the density of the polymeric solutions to be 1000 kg m^{-3} throughout the present work.

Characterization of the viscoelastic behaviour of the solutions is done by conducting rheology experiments on Anton

Table 1 Molecular weight of the polymers and time taken to prepare the solutions

Polymer	Supplier	Molecular weight (g mol^{-1})	Stirring time
PAM	Himedia chemical Co.	5 000 000	12 h
PEO	Sigma-Aldrich chemical Co.	4 000 000	24 h
PVA	Sigma-Aldrich chemical Co.	90 000	0.5 h at 90 °C and 6 h at 40 °C
PEG	Sigma-Aldrich chemical Co.	10 000	6 h

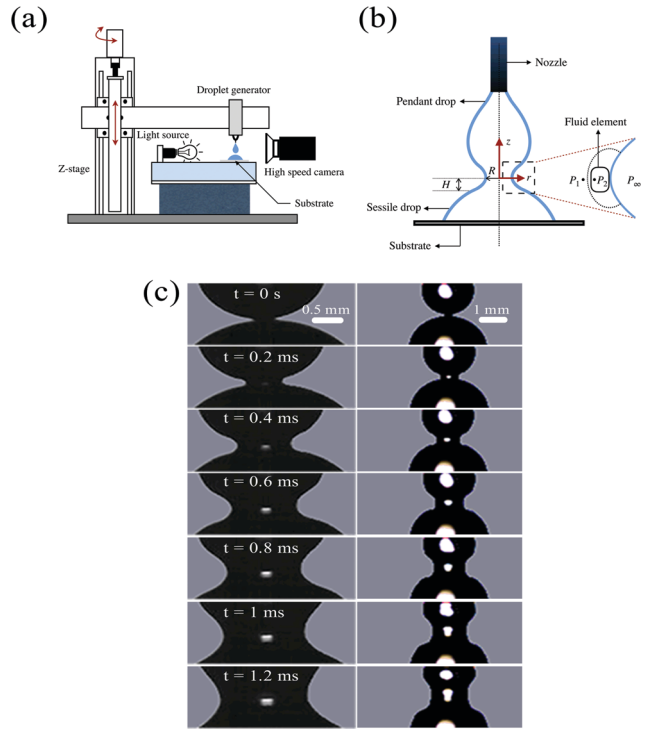

Fig. 1 (a) Schematic of the experimental setup, (b) Schematic of neck region during coalescence, (c) neck radius evolution of 0.5% w/v concentration of PEO on the left compared with DI water on the right at different instants.

Paar MCR 302 rheometer using a cone and plate 40 mm, 1° geometry. Parameters governing viscoelastic behaviour such as shear viscosity η, critical concentration c^*, intrinsic viscosity $[\eta]$ and relaxation time λ are obtained by using the relations[51–54] for the polymer solutions and are given Table 2 with detailed calculations in ESI.†

Table 2 Characterization of fluid properties using Anton-Paar MCR-302 with cone and plate 40 mm, 1° geometry for viscosity. Surface tension values are obtained using Dataphysics OCA25 Optical contact angle measuring and contour analysis systems using pendant drop method

Polymer	c (%w/v)	c^* (%w/v)	c/c^*	λ (ms)	η (Pa s)	σ (mN m)
PAM	0.01%	0.06%	0.17	1.1	0.006	71 ± 2
	0.02%		0.33	1.1	0.013	71 ± 2
	0.04%		0.67	1.1	0.028	71 ± 2
	0.05%		0.83	1.1	0.035	71 ± 2
	0.06%		1	1.1	0.043	71 ± 2
	0.2%		3.3	1.67	0.146	71 ± 2
	0.3%		5	1.93	0.258	71 ± 2
	0.4%		6.7	2.14	0.329	71 ± 2
	0.5%		8.3	2.315	0.439	71 ± 2
	0.6%		10	55.13	0.509	71 ± 2
PEO	0.2%	0.071%	2.82	1.833	0.009	62 ± 2
	0.3%		4.23	2.28	0.015	62 ± 2
	0.4%		5.63	2.63	0.018	62 ± 2
	0.5%		7.04	52	0.038	62 ± 2
	0.6%		8.45	74	0.052	62 ± 2
PVA	0.2%	1.21%	0.17	1.5×10^{-3}	0.00128	54 ± 2
	0.3%		0.25	1.5×10^{-3}	0.00154	52 ± 2
	0.4%		0.33	1.5×10^{-3}	0.00171	48 ± 1
	0.5%		0.42	1.5×10^{-3}	0.00182	48 ± 2
	0.6%		0.5	1.5×10^{-3}	0.00192	48 ± 2
PEG	0.2%	5.3%	0.037	30×10^{-6}	0.00124	63 ± 1
	0.3%		0.057	30×10^{-6}	0.00127	62 ± 1
	0.4%		0.075	30×10^{-6}	0.00131	61 ± 1
	0.5%		0.094	30×10^{-6}	0.00135	59 ± 1
	0.6%		0.113	30×10^{-6}	0.00141	59 ± 1
	8%		1.51	34.65×10^{-6}	0.0048	56 ± 1
	12%		2.26	39.91×10^{-6}	0.0097	54 ± 1
	16%		3.01	44.11×10^{-6}	0.0125	53 ± 1
	20%		3.77	48.95×10^{-6}	0.0178	52 ± 1[a]
	24%		4.52	52.34×10^{-6}	0.0241	51 ± 1

[a] Represents interpolated value.

3 Results

Coalescence of a hanging pendant drop with a sessile drop proceeds *via* the formation of a liquid bridge, where the neck radius R varies with time; see Fig. 1b. The kinematics of such a configuration is similar to hanging drop coalescence and proceeds with a radially symmetric liquid bridge. It is different from the coalescence of spreading drops in which the substrate plays an important role leading to a radially asymmetric liquid bridge. Such evolution of the liquid bridge during coalescence of an aqueous solution of 0.5% w/v PEO and DI water at different time instants are shown in Fig. 1c. These figures are accompanied by a schematic of the neck region, depicting the geometric parameters H and R as the two pertinent length scales associated with neck geometry, R_o being the radius of the drop. As a representative scenario, the temporal evolution of the neck radius during coalescence is shown for the chosen polymeric liquids at 0.5% w/v concentration, along with that for DI water as a control case, as depicted in Fig. 2. For PAM and PEO solutions, the Weissenberg number, which is defined as the ratio of elastic forces and viscous forces given by $\mathrm{Wi} = \lambda U/R$ (λ is relaxation time of the fluid, U is scaled as the neck velocity

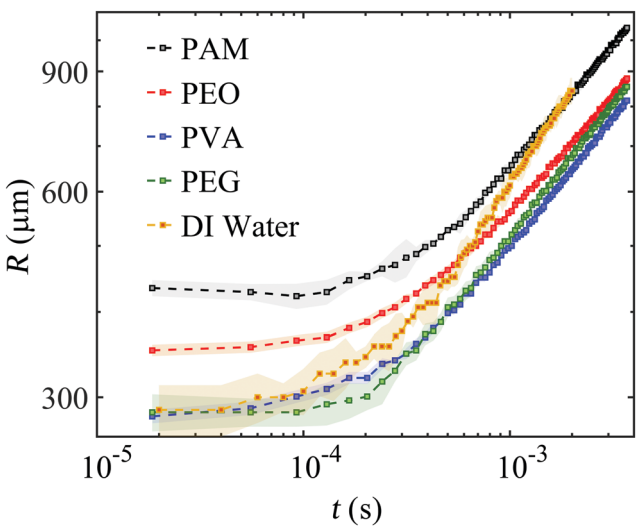

Fig. 2 Temporal evolution of neck radius with time during the merging of 0.5% w/v concentration of polymer solutions: PAM, PEO, PVA, PEG, and DI Water with shades representing the standard deviation.

and R as the neck radius), is of $\mathcal{O}(1)$, suggesting that both elastic and viscous forces are comparable and are governing the coalescence phenomenon, resulting in the slope of temporal neck radius evolution as 0.36 ± 0.02 as observed in Fig. 2. In the same figure, PVA and PEG follow an altered slope of neck radius evolution as 0.39 ± 0.02, wherein the Weissenberg number is of $\mathcal{O}(10^{-3}-10^{-4})$, suggesting the dominance of viscous forces. This signifies a shift towards Newtonian behaviour which has a slope of 0.5. Such comparison of elastic forces and viscous forces is shown in the form of a variation in storage modulus G' and loss modulus G'' with shear strain γ for 0.3% w/v PEO and 24% w/v PEG in Fig. S3a (see ESI†). We also demonstrate a similar variation of G' and G'' with angular frequency ω for two typical concentrations 0.4% w/v and 0.6% w/v for PEO in Fig. S3b (see ESI†). The higher difference between G' and G'' values for PEG as contrasted with PEO further strengthens the claim of increased Newtonian behaviour with a reduced elastic component.

To explore a possible universality in the coalescence dynamics, one may first appeal to the intrinsic rheology of the polymeric fluids. The elastic behaviour of these polymer solutions is quantified by the relaxation time λ that may be estimated by employing the Zimm model.[45] The values of the relaxation time of the chosen polymeric solutions are listed in Table 2. The polymeric fluids are characteristically shear thinning in nature.[45] Fig. 3a shows the variation of η as a function of shear rate $\dot{\gamma}$ for PAM, PEO, and PEG solutions for concentration values such that $c/c^* > 1$, and indicates shear thinning behaviour for PAM and PEO. However, a weak dependence of viscosity on the shear rate is observed for PEG. Fig. 3b brings out similar trends as Fig. 3a for PAM, PVA and PEG solutions for concentration values such that $c/c^* < 1$, and shows the shear-thinning behaviour for PAM, whereas weak dependence of viscosity on the shear rate is observed for PVA and PEG. This can be extended for all the concentrations of the above polymers which have $c/c^* < 1$. The viscosity curves for all the solutions are provided in Fig. S2 of ESI.†

Similarity in trends of temporal variation of neck radius, as portrayed in Fig. 2, suggested a universal scaling. To determine the functional form of the dynamic evolution of the normalized neck radius, we first note that the characteristic length scale R_c and the characteristic time scale t_c obtained from scaling of surface tension, inertial and elastic forces as represented in eqn (1) and (2). Here, the effect of gravitational force is neglected on the basis of Bond number: $\mathrm{Bo} = \rho g {R_o}^2/\sigma$, which is of $\mathcal{O}(10^{-1})$ in the present study.

$$\lambda \eta A \dot{\gamma}^2 \sim \sigma R_o \quad (1)$$

$$\rho A U^2 \sim \sigma R_o \quad (2)$$

Here, U represents the characteristic velocity, A represents characteristic area in which flow is predominant. The characteristic length scale $R_c = \sqrt{\nu_o \lambda}$ and characteristic time scale $t_c = \mathrm{Oh}\lambda$ (where, ν_o is the kinematic viscosity, λ is the relaxation time of the solution and $\mathrm{Oh} = \eta/\sqrt{R_o \rho \sigma}$ is the Ohnesorge number) are obtained from eqn (1) and (2) from a competitive

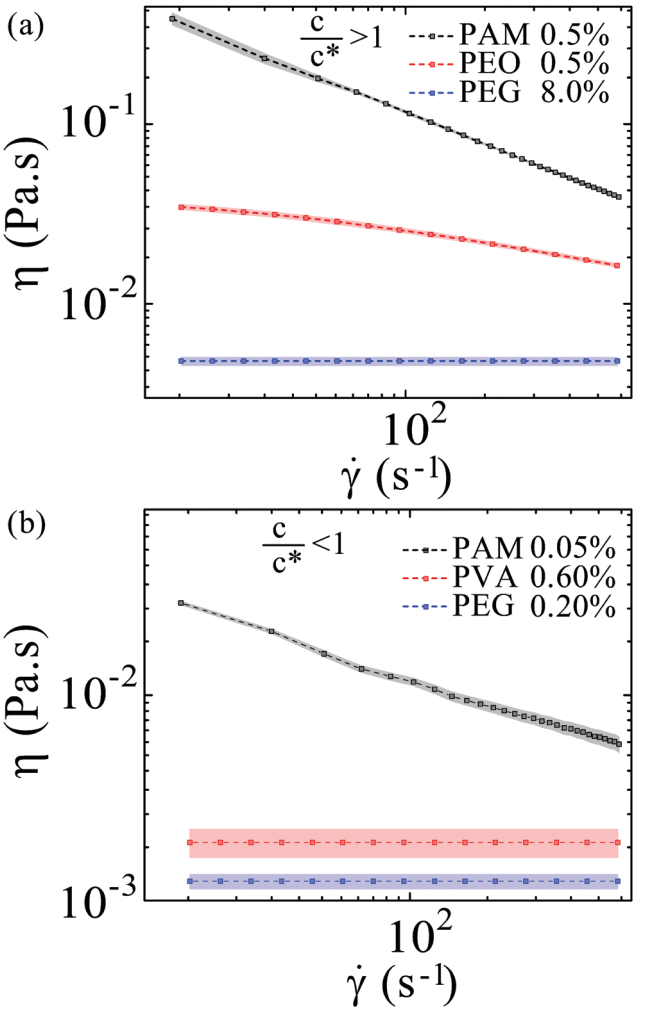

Fig. 3 Rheological behaviour of (a) PAM, PEO and PEG of concentrations 0.5% w/v, 0.5% w/v and 8% w/v respectively having $c/c^* > 1$, (b) PAM, PVA and PEG of concentrations 0.05% w/v, 0.6% w/v and 0.2% w/v respectively such that $c/c^* < 1$ with representation of standard deviation using shades.

balance of pertinent forces. By representing the experimental data in terms of these normalized variables, the variation of dimensionless radius $\left(R^* = \frac{R}{\sqrt{\nu_o \lambda}}\right)$ with dimensionless time $\left(t^* = \frac{t}{\lambda}\mathrm{Oh}^{-1}\right)$ assumes the following generic functional form given in eqn (3). The concentration ratio c/c^* is empirically added in the form of $(c/c^*)^{-1.2}$ to the non-dimensional time, by observing R^* *vs.* t^* variation, to get the universal scaling.

$$R^* = f\left(\frac{t}{\lambda}\mathrm{Oh}^{-1}, \frac{c}{c^*}\right) \quad (3)$$

The collapse of data into a universal characteristic is depicted in Fig. 4. Following this figure, it can be inferred that when the dimensionless radius is scaled with $\left(\frac{t}{\lambda}\mathrm{Oh}^{-1}\right)\left(\frac{c}{c^*}\right)^{-1.2}$

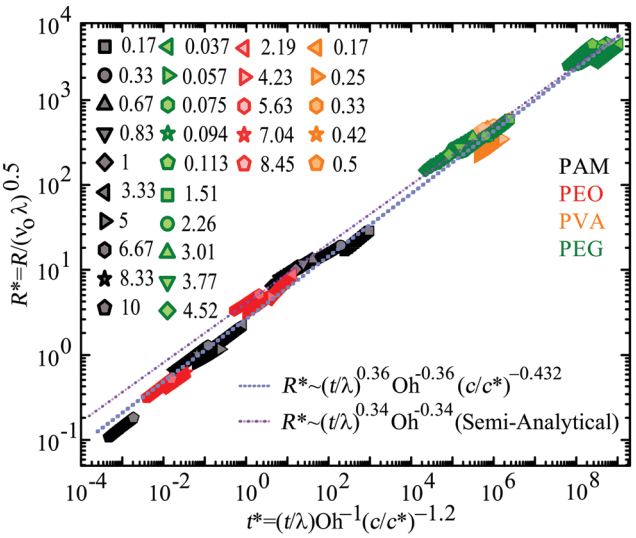

Fig. 4 Scaling of non-dimensionalized neck radius as function of non-dimensional time with legend representing the values of c/c^* of all the polymer solutions used in the study.

one may arrive at a universal correlation given in eqn (4)

$$R^* \sim \left(\frac{t}{\lambda}\right)^{0.36}\left(\frac{c}{c^*}\right)^{-0.432}\mathrm{Oh}^{-0.36} \tag{4}$$

The scaling law proposed above may be verified from a rigorous theoretical perspective as well. For illustration, without sacrificing generality, one may take the example of the special case of $\frac{c}{c^*} = 1$. We appeal to the linear Phan-Thien-Tanner (PTT) model for viscoelastic rheology as represented in eqn (5) to obtain the relation between stress and rate of deformation,

$$\lambda \overset{\nabla}{\boldsymbol{\tau}} + \boldsymbol{\tau}\left[1 + \frac{\kappa\lambda}{\eta}\mathrm{Tr}(\boldsymbol{\tau})\right] = 2\eta \boldsymbol{D} \tag{5}$$

where, $\boldsymbol{\tau}$ is the stress tensor, κ is a constant and $\boldsymbol{D}$ is deformation rate tensor.

Assuming the flow as quasi-steady and quasi-radial, the conservation of mass and momentum equation in the radial direction are reduced to eqn (6) and (7) respectively.

$$\frac{\partial \nu_r}{\partial r} + \frac{\partial \nu_z}{\partial z} + \frac{\nu_r}{r} = 0 \tag{6}$$

$$\rho \nu_r \frac{\partial \nu_r}{\partial r} = -\frac{\partial p}{\partial r} + \frac{\tau_{rr}}{r} + \frac{\partial \tau_{rr}}{\partial r} + \frac{\partial \tau_{rz}}{\partial z} \tag{7}$$

Various parameters appearing in eqn (5)–(7) are scaled as, $\boldsymbol{\tau} \to \mathrm{Wi}\bar{\boldsymbol{\tau}}$; $p \to \mathrm{Wi}\bar{p}$; $R \to \bar{R}/\sqrt{\mathrm{Wi}}$; $U \to \sqrt{\mathrm{Wi}}\bar{U}$ (p is pressure, U is average velocity of neck radius and the quantities represented with bars are scaled parameters and Wi is the Weissenberg number). Using the approximations given in eqn (8) and (9), the scaled stresses are estimated as eqn (10) and (11)

$$\lambda \mathrm{Wi}^2 \ll 1 \tag{8}$$

$$1 + \frac{\kappa\lambda\mathrm{Wi}}{\eta}\bar{\boldsymbol{\tau}} \sim \frac{\kappa\lambda\mathrm{Wi}}{\eta}\bar{\boldsymbol{\tau}} \tag{9}$$

$$\tau_{rr} \sim \sqrt{2\eta^2/\kappa\lambda}\sqrt{\partial \nu_r/\partial r} \tag{10}$$

$$\tau_{rz} = \tau_{rr}\left(\frac{\partial \nu_r}{\partial z}\right)\Big/\left(2\frac{\partial \nu_r}{\partial r}\right). \tag{11}$$

By introducing the scaling arguments: $\nu_r \sim U$, $r \sim R$, $z \sim R$ into the momentum equation, considering the characteristic differential pressure ΔP as the Laplace pressure, along with the geometric constraint eqn (12) obtained from Fig. 1a, one may obtain eqn (13) with c_1 and c_2 as scaling constants.

$$\frac{H}{R} \approx \frac{R}{2R_o} \tag{12}$$

$$\rho U^2 = c_1\frac{2\sigma R_o}{R^2} - c_2\sqrt{\frac{2\eta^2}{\kappa\lambda}}\frac{\sqrt{U}}{\sqrt{R}} \tag{13}$$

Towards arriving at this, the inside and the outside pressures, P_1 and P_2 respectively, are estimated as: $P_1 - P_\infty = \frac{2\sigma}{R_o}$, $P_2 - P_\infty = \sigma\left(\frac{1}{H} + \frac{1}{R}\right)$ (P_∞ being the atmospheric pressure). Further, introduction of the dimensionless parameters: $R^* = R/\sqrt{\nu_o\lambda}$ and $t^* = t/\mathrm{Oh}\lambda$, leads to

$$\left(\frac{\mathrm{d}R^*}{\mathrm{d}t^*}\right)^2 + \frac{A_1}{\sqrt{R^*}}\left(\frac{\mathrm{d}R^*}{\mathrm{d}t^*}\right)^{\frac{1}{2}} - \frac{A_2}{R^{*2}} = 0 \tag{14}$$

where, $A_1 = \frac{\sqrt{2}}{\sqrt{\kappa}}c_2\mathrm{Oh}^{\frac{3}{2}}$ and $A_2 = \frac{2c_1\sigma R_o}{\rho{\nu_o}^2}\mathrm{Oh}^2$. We obtain the solution of eqn (14) using the initial condition $R^*(0) = \Phi$, where $\Phi \to 0^+$ is a sufficiently small value enabling the convergence of the numerical solution and emulate the radius of the nascent droplet bridge. The numerical solution of eqn (14) fits to the following functional form: $R^* \propto (t^*)^{0.34}$. This theoretically obtained characteristic is compared with the experimental variation: $R^* \propto (t^*)^{0.36}$ in Fig. 4. This close agreement clearly rationalizes the experimental data from a fundamental theoretical perspective.

For a Newtonian fluid, the nondimensional neck radius ${R_1}^* = R/\mathrm{Oh}D_o$ and nondimensional time ${t_1}^* = t\sigma/\eta\mathrm{Oh}D_o$ results in the scaling of ${R_1}^* \propto {t_1}^{*0.5}$ in the inertial regime.[42] Such scaling for DI water is shown in Fig. S1 in ESI,† for the inertial regime. However, for the polymeric fluids the neck radius growth has been delayed compared to water which is represented by the exponent 0.36 in contrast to the Newtonian fluid. The empirically added concentration ratio in t^* leads to the overall dependency of R^* with c/c^* with an exponent of −0.432.

4 Conclusions

The unveiling of a hitherto unknown dynamical map for coalescing polymeric fluids, which we term rheocoalescence, opens up a new outlook in understanding the governing law behind neck-radius evolution of such a phenomenon, which in turn, can give cues to answering complex questions

in physiological fluid dynamics. These studies can be extended to wider varieties of viscoelastic fluids bearing further implications to emerging industrial applications on emulsion-based technologies and microfluidics. The scaling laws proposed by previous studies of drop coalescence for Newtonian fluids are not valid here. In ref. 28, it has been reported that $R_c = \eta^2/\rho\sigma$ and $t_c = \eta^3/\rho\sigma^2$, whereas $t_c = \eta R_o/\sigma$ was postulated in ref. 24. In ref. 31, it has been reported that $t_c = \sqrt{\eta R_o^3/\sigma}$. We have also confirmed that[42] $R_c = \mathrm{Oh}D_o$ and $t_c = \eta \mathrm{Oh} D_o/\sigma$ taking DI water as a Newtonian fluid. We have extended the importance of Oh as an important non-dimensional number for polymeric fluids through the inclusion of λ in the characteristic scales to hallmark the distinction of a polymeric fluid. This shows the stark difference from the scaling laws for Newtonian droplets. The present scaling law elegantly captures the universality of coalescence of simple polymeric fluids with surrounding fluid as air through the accretion of the liquid bridge as it expands radially. From a broader perspective, the exploration of how the topographical evolutions and the relevant spatio-temporal scales mediate droplet coalescence dynamics for complex fluids represents an important advance in our understanding of their dynamical characteristics, which will enable the rationalization and emergence of a plethora of applications guided by the unified scaling law. This, however, requires further exploration on the domain of it's applicability. The inclusion of other non-Newtonian fluids, such as polymeric blends and polymer melts, into the ambit of the postulated scaling law needs further investigation.

5 Summary

In summary, we have experimentally and analytically investigated the coalescence of polymeric liquid drops. It has been observed that the scaling laws proposed by previous studies on drop coalescence for Newtonian fluid are not valid in the coalescence of viscoelastic liquids. We showed that the variation of non-dimensional neck radius depends on non-dimensional time, where both the relaxation time scale and concentration of the polymer play a role. Finally, we proposed a universal scaling for neck radius, which depends on viscoelastic properties of the polymer solutions.

Conflicts of interest

There are no conflicts to declare.

Acknowledgements

S. C. acknowledges Department of Science and Technology, Government of India, for Sir J. C. Bose National Fellowship, A. K. acknowledges support from DST-SERB grant no. EMR/2017/003025.

Notes and references

1 E. Villermaux and B. Bossa, *Nat. Phys.*, 2009, **5**, 697.
2 E. Bowen, *Aust. J. Chem.*, 1950, **3**, 193–213.
3 H. R. Pruppacher and J. D. Klett, *Microphysics of Clouds and Precipitation*, Springer, 2010, pp. 10–73.
4 A. Kovetz and B. Olund, *J. Atmos. Sci.*, 1969, **26**, 1060–1065.
5 N. Ashgriz and J. Poo, *J. Fluid Mech.*, 1990, **221**, 183–204.
6 H. Djohari, J. I. Martnez-Herrera and J. J. Derby, *Chem. Eng. Sci.*, 2009, **64**, 3799–3809.
7 K. Rykaczewski, J. H. J. Scott, S. Rajauria, J. Chinn, A. M. Chinn and W. Jones, *Soft Matter*, 2011, **7**, 8749–8752.
8 A. D. Barbosa, D. B. Savage and S. Siniossoglou, *Curr. Opin. Cell Biol.*, 2015, **35**, 91–97.
9 A. R. Thiam, R. V. Farese Jr and T. C. Walther, *Nat. Rev. Mol. Cell Biol.*, 2013, **14**, 775–786.
10 A. R. Thiam and L. Forêt, *Biochim. Biophys. Acta, Mol. Cell Biol. Lipids*, 2016, **1861**, 715–722.
11 F. Wilfling, J. T. Haas, T. C. Walther and R. V. Farese Jr, *Curr. Opin. Cell Biol.*, 2014, **29**, 39–45.
12 P. L. Smith, D. J. Musil, A. G. Detwiler and R. Ramachandran, *J. Appl. Meteorol.*, 1999, **38**, 145–155.
13 K. Mahdi, R. Gheshlaghi, G. Zahedi and A. Lohi, *J. Pet. Sci. Eng.*, 2008, **61**, 116–123.
14 S. Stewart and G. Mazza, *J. Food Qual.*, 2000, **23**, 373–390.
15 M. Orme, *Prog. Energy Combust. Sci.*, 1997, **23**, 65–79.
16 O. Pitois, P. Moucheront and X. Chateau, *J. Colloid Interface Sci.*, 2000, **231**, 26–31.
17 C. Klopp, R. Stannarius and T. Trittel, *Soft Matter*, 2020, **16**, 4607–4614.
18 A. B. Pawar, M. Caggioni, R. Ergun, R. W. Hartel and P. T. Spicer, *Soft Matter*, 2011, **7**, 7710–7716.
19 H. Fan and A. Striolo, *Soft Matter*, 2012, **8**, 9533–9538.
20 C. P. Whitby and M. Krebsz, *Soft Matter*, 2014, **10**, 4848–4854.
21 H. Zeng, B. Zhao, Y. Tian, M. Tirrell, L. G. Leal and J. N. Israelachvili, *Soft Matter*, 2007, **3**, 88–93.
22 S. Vandebril, J. Vermant and P. Moldenaers, *Soft Matter*, 2010, **6**, 3353–3362.
23 T. Krebs, K. Schroën and R. Boom, *Soft Matter*, 2012, **8**, 10650–10657.
24 J. Eggers, J. R. Lister and H. A. Stone, *J. Fluid Mech.*, 1999, **401**, 293–310.
25 M. Wu, T. Cubaud and C.-M. Ho, *Phys. Fluids*, 2004, **16**, L51–L54.
26 J. D. Paulsen, J. C. Burton and S. R. Nagel, *Phys. Rev. Lett.*, 2011, **106**, 114501.
27 J. D. Paulsen, J. C. Burton, S. R. Nagel, S. Appathurai, M. T. Harris and O. A. Basaran, *Proc. Natl. Acad. Sci. U. S. A.*, 2012, **109**, 6857–6861.
28 D. G. Aarts, H. N. Lekkerkerker, H. Guo, G. H. Wegdam and D. Bonn, *Phys. Rev. Lett.*, 2005, **95**, 164503.
29 F. Blanchette and T. P. Bigioni, *Nat. Phys.*, 2006, **2**, 254.
30 S. C. Case and S. R. Nagel, *Phys. Rev. Lett.*, 2008, **100**, 084503.
31 L. Duchemin, J. Eggers and C. Josserand, *J. Fluid Mech.*, 2003, **487**, 167–178.
32 R. W. Hopper, *J. Am. Ceram. Soc.*, 1984, **67**, C-262.
33 R. W. Hopper, *J. Fluid Mech.*, 1990, **213**, 349–375.

34 J. D. Paulsen, *Phys. Rev. E: Stat., Nonlinear, Soft Matter Phys.*, 2013, **88**, 063010.
35 J. D. Paulsen, R. Carmigniani, A. Kannan, J. C. Burton and S. R. Nagel, *Nat. Commun.*, 2014, **5**, 3182.
36 W. Ristenpart, P. McCalla, R. Roy and H. A. Stone, *Phys. Rev. Lett.*, 2006, **97**, 064501.
37 W. Yao, H. Maris, P. Pennington and G. Seidel, *Phys. Rev. E: Stat., Nonlinear, Soft Matter Phys.*, 2005, **71**, 016309.
38 S. Decent, G. Sharpe, A. Shaw and P. Suckling, *Int. J. Multiphase Flow*, 2006, 32, 717–738.
39 M. Gross, I. Steinbach, D. Raabe and F. Varnik, *Phys. Fluids*, 2013, **25**, 052101.
40 J. Sprittles and Y. Shikhmurzaev, *Phys. Fluids*, 2012, **24**, 122105.
41 S. T. Thoroddsen and K. Takehara, *Phys. Fluids*, 2000, **12**, 1265–1267.
42 X. Xia, C. He and P. Zhang, *Proc. Natl. Acad. Sci. U. S. A.*, 2019, **116**, 23467–23472.
43 R. W. Hopper, *J. Am. Ceram. Soc.*, 1993, **76**, 2947–2952.
44 R. W. Hopper, *J. Am. Ceram. Soc.*, 1993, **76**, 2953–2960.
45 R. B. Bird, R. C. Armstrong and O. Hassager, 1987.
46 R. I. Tanner and S. Nasseri, *J. Non-Newtonian Fluid Mech.*, 2003, **116**, 1–17.
47 A. V. Dobrynin, R. H. Colby and M. Rubinstein, *Macromolecules*, 1995, **28**, 1859–1871.
48 R. H. Colby, M. Rubinstein and M. Daoud, *J. Phys. II*, 1994, **4**, 1299–1310.
49 Y. Liu, Y. Jun and V. Steinberg, *J. Rheol.*, 2009, **53**, 1069–1085.
50 O. Arnolds, H. Buggisch, D. Sachsenheimer and N. Willenbacher, *Rheol. Acta*, 2010, **49**, 1207–1217.
51 J. Francois, D. Sarazin, T. Schwartz and G. Weill, *Polymer*, 1979, **20**, 969–975.
52 I. Lamatic, M. Bercea and S. Morariu, *Rev. Roum. Chim.*, 2009, **54**, 981–986.
53 J. Lee and A. Tripathi, *Anal. Chem.*, 2005, **77**, 7137–7147.
54 V. Tirtaatmadja, G. H. McKinley and J. J. Cooper-White, *Phys. Fluids*, 2006, **18**, 043101.